Vortex Phase Diagram in Rotating Two-Component Bose-Einstein Condensates

Kenichi Kasamatsu,[1] Makoto Tsubota,[1] and Masahito Ueda[2]

[1]*Department of Physics, Osaka City University, Sumiyoshi-Ku, Osaka 558-8585, Japan*
[2]*Department of Physics, Tokyo Institute of Technology, Meguro-ku, Tokyo 152-8551, Japan*
(Received 7 March 2003; published 10 October 2003)

We investigate the structure of vortex states in rotating two-component Bose-Einstein condensates with equal intracomponent but varying intercomponent-coupling constants. A phase diagram in the intercomponent-coupling versus rotation-frequency plane reveals rich equilibrium structures of vortex states. As the ratio of intercomponent to intracomponent couplings increases, the interlocked vortex lattices undergo phase transitions from triangular to square, to double-core lattices, and eventually develop interwoven "serpentine" vortex sheets with each component made up of chains of singly quantized vortices.

A system described by a multicomponent order parameter can excite various exotic topological defects. There has been great interest in the study of such topological defects, which have been explored extensively in condensed matter systems such as anisotropic superfluid ^{3}He [1]. This study is also closely related with some problems in superconductors of UPt_3 and Sr_2RuO_4 which are thought to have non-s-wave symmetry [2] and high-energy physics and cosmology [3]. Dilute atomic Bose-Einstein condensates (BECs) offer another superior testing ground to investigate the physics of exotic topological defects because they are free from impurities and well controlled by optical techniques. A trapped BEC in a rotating potential generates quantized vortices which are topological defects characteristic of superfluidity, and several groups have succeeded in observing ordered vortex lattices [4]. While many interesting phenomena have been found in single-component BECs [4], a rich variety of static and dynamic phenomena are expected to occur in a system of rotating two-component BECs consisting, for example, of two different hyperfine spin states of atoms [5]. This system is characterized by three coupling constants denoted by C_{11} and C_{22} (for intracomponents) and C_{12} (for intercomponent) [6–10]. In this Letter, we report equilibrium structures of vortex states in two-component BECs with $C_{11} = C_{22} \equiv C$ but varying values of C_{12} and the rotation-frequency based on the numerical analysis of the Gross-Pitaevskii equation.

Mueller and Ho studied the vortex lattice structure of two-component BECs by assuming the lowest Landau level approximation and a perfect lattice [11]. They proposed a phase diagram on the lattice structure and found that, as C_{12}/C is increased, the system undergoes a continuous structural change from triangular to square lattices. Kita *et al.* discussed the lattice structure in $F = 1$ spinor BECs [12]. However, both studies assume the fast rotation limit where the rotation-frequency is very close to the radial trapping frequency, so a vast experimentally accessible parameter regime remains to be ex-

plored. When there is no rotation, it is known that we obtain miscible condensates as the ground state for $C_{12}/C < 1$, while for $C_{12}/C > 1$ the two components phase separate [6,7,10]. In the presence of rotation, our numerical analysis reveals a rich variety of vortex states which have eluded analytic treatments. In particular, we find that for $C_{12}/C \geq 1$ double-core vortex lattices or interwoven serpentine vortex sheets become stabilized for a considerable range of rotation frequency; these states can therefore be observed in current experimental situations.

The equilibrium solutions of two-component BECs in a frame rotating with the angular velocity $\mathbf{\Omega} = \Omega\hat{\mathbf{z}}$ are obtained by solving the time-independent coupled Gross-Pitaevskii (GP) equations for the condensate wave functions $(h_i + \sum_{j=1,2} C_{ij}|\Psi_j|^2)\Psi_i = \mu_i\Psi_i$ ($i = 1, 2$) [6–10] where $h_i = -(m_{12}/m_i)\nabla^2 + V_i - (\Omega/\bar{\omega})L_z$ with the reduced mass $m_{12} = m_1m_2/(m_1 + m_2)$ and the harmonic potential $V_i = (m_i\omega_i^2/4m_{12}\bar{\omega}^2)r^2$. Here, length and energy are measured in units of $b_{ho} = \sqrt{\hbar/2m_{12}\bar{\omega}}$ and $\hbar\bar{\omega} \equiv \hbar(\omega_1 + \omega_2)/2$, respectively. In this work, the numerical calculation is done in the two-dimensional x-y space. The wave functions are normalized as $\int dx\,dy|\Psi_i(x, y)|^2 = 1$ and, then, the intracomponent and intercomponent-coupling constants are written as $C_{ii} = 8\pi(m_{12}/m_i)N_i^{2D}a_{ii}$ and $C_{ij} = 4\pi N_j^{2D}a_{12}$ ($i \neq j$) with the corresponding s-wave scattering lengths a_{11}, a_{22}, a_{12} (assumed to be positive), and the particle numbers N_i^{2D} per unit length along the z axis.

For simplicity, the number of the parameters is reduced by assuming $a_{11} = a_{22}$, $m_1 = m_2$, $\omega_1 = \omega_2 = \bar{\omega}$, and $N_1^{2D} = N_2^{2D} = N^{2D}$. For the typical experimental conditions $(\omega_\perp, \omega_z) = 2\pi(8, 5)$ Hz and $N \sim 10^6$, the values of the intracomponent coupling constants are chosen as $C_{11} = C_{22} = C = 2000$. In the numerical calculation, the equilibrium solutions are found by the norm-preserving imaginary time propagation of the time-dependent coupled GP equations, starting from arbitrary trial wave functions without vorticity. The

propagation continues until the fluctuation in the norm of the wave function becomes smaller than 10^{-8}.

With a fixed value $C = 2000$, we investigate the equilibrium solutions for various values of two free parameters $\delta \equiv C_{12}/C$ and $\bar{\Omega} \equiv \Omega/\bar{\omega}$. The obtained vortex structure is summarized in the phase diagram of Fig. 1. Because the centrifugal potential overcomes the harmonic trapping potential for $\bar{\Omega} > 1$, the upper limit of the rotation frequency is set by $\bar{\Omega} = 1$. Previous studies have revealed that two nonrotating components with equal mass and equal intracomponent scattering length overlap completely for $\delta < 1$, and phase separate for $\delta > 1$ [6,7,10]. This criterion is reflected on the structure of vortex states, as explained below. In general, there are many metastable states in rotating two-component BECs; they are obtained by the numerical simulation starting from different wave functions. Here we discuss some characteristic features of vortex structures.

In the region $\delta < 1$, two types of the regular vortex lattices are obtained as the equilibrium state. For $\delta = 0$, where two components are not interacting, the formulation is equivalent to that of one component, thereby triangular vortex lattices are formed [13]. As δ increases, the positions of vortex cores in one component gradually shift from those of the other component and the triangular lattices are distorted. Eventually, the vortices in each component form a square lattice rather than a triangular one. The δ dependence on the stable region of a square lattice was studied in Ref. [11] in the high rotation limit $\bar{\Omega} \simeq 1$. As seen in Fig. 1, however, that stable region depends not only on δ but also sensitively on $\bar{\Omega}$. An increase in rotation frequency also causes the transition from triangular to square lattices; in Figs. 2(a) and 2(b), the two-dimensional density profiles of the condensates with $\delta = 0.7$ are shown for $\bar{\Omega} = 0.6$ and $\bar{\Omega} = 0.75$. We find that the two vortex lattices are interlocked in such a manner that a peak in the density of one component is located at the density hole of the other, as shown in Fig. 2(c). As a result, the total density $\rho_T = |\Psi_1|^2 + |\Psi_2|^2$ obeys the Thomas-Fermi distribution applied to the overlapping two-component BECs with solid-body rotation $\rho_T(r) = 2\sqrt{\alpha/\pi} - \alpha r^2$ with $\alpha = (1 - \bar{\Omega}^2)/C(1 + \delta)$. We have confirmed that this feature holds for other parameter regimes.

Why is the square lattice stabilized in two-component BECs? According to the energy functional of this system, two components interact via the intercomponent interaction $C_{12}|\Psi_1|^2|\Psi_2|^2$; the velocity field in one component is independent of that of the other. Therefore, such a feature is determined only by the density distribution of the condensates which minimizes the interaction energy. We rewrite the interaction energy in terms of the total density ρ_T and the "spin" variable $S = |\Psi_1|^2 - |\Psi_2|^2$ as
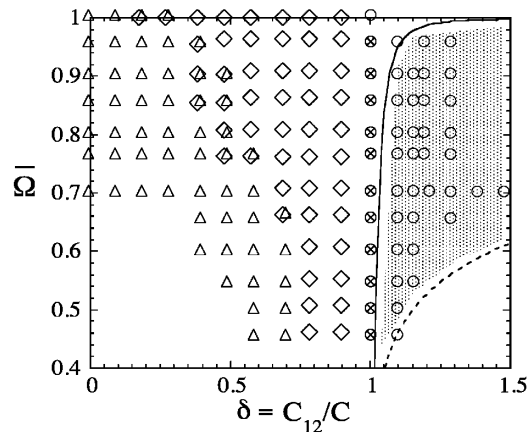

FIG. 1. $\bar{\Omega}$-δ phase diagram of the vortex states in rotating two-component BECs. The classification of the structure is made by the following symbols: $\triangle$, triangular lattice; $\diamond$, square lattice; $\otimes$, stripe or double-core vortex lattice; $\bigcirc$, vortex sheet. Because of the continuous change from triangular to square, their boundary is shown by using both $\triangle$ and $\diamond$. The plots at $\bar{\Omega} = 1$ show the results of Ref. [11]. The shaded region shows the analytically obtained region of vortex sheets; the solid curve represents $b = \Lambda_p$ and the dashed curve $2b = R_{\mathrm{TF}}$ (see text).
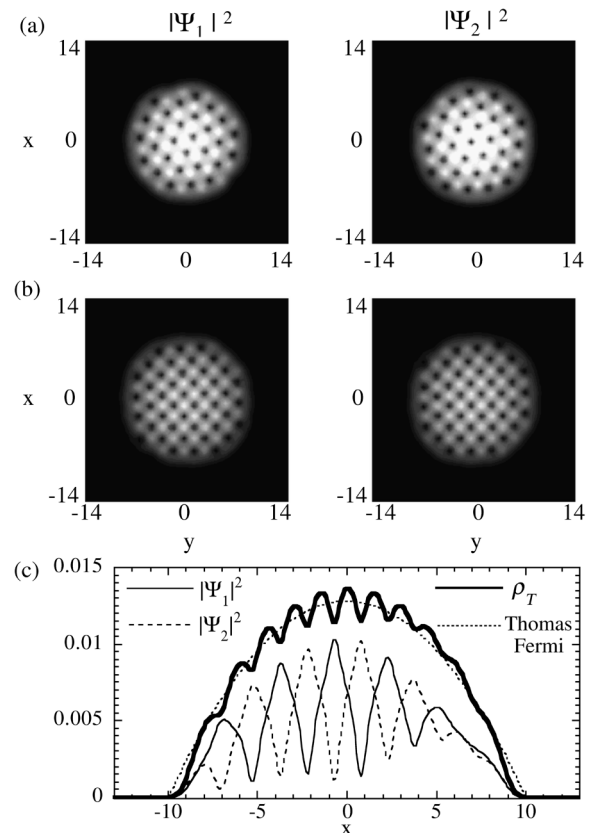

FIG. 2. Two-dimensional density profile of the condensates with $C = 2000$ and $\delta = 0.7$ for (a) $\bar{\Omega} = 0.6$ and (b) $\bar{\Omega} = 0.75$. (c) Cross section of (b) along the $y = 0$ line. The total density $\rho_T = |\Psi_1|^2 + |\Psi_2|^2$ and the Thomas-Fermi density profile are also shown.

$E_{int} = \int d\mathbf{r} C[(1 + \delta)\rho_T^2 + (1 - \delta)S^2]/4$. A larger δ makes a smoother total density ρ_T more favorable in order to reduce the first term of E_{int}. This results in the shift of the positions of vortex cores of each component. Then, the last term of E_{int} can be interpreted effectively as the interaction energy between spins in the Ising model [14]. Spin-up components correspond to the density peaks of Ψ_1 at the vortex cores of Ψ_2, and vice versa for spin-down components. When the coefficient $1 - \delta$ is positive, the interaction between spins is antiferromagnetic, which makes a square lattice stabilized (because the triangular lattice could be frustrated). The antiferromagnetic nature is made more pronounced as the interlocking of vortex lattices becomes stronger with δ and the number of vortices increase with $\bar{\Omega}$.

As δ exceeds unity, the system enters a ferromagnetic phase. Then, the condensates undergo phase separation to spontaneously form domains having the same spin component [14]. Concurrently, vortices of the same component begin to overlap at $\delta \sim 1$. Figure 3 shows typical solutions at $\delta = 1$. In Fig. 3(a), vortices of each component are overlapped in lines, and each condensate density forms a stripe pattern [15]. While this structure can also be derived if one assumes a perfect lattice [11], we find that its energy is nearly degenerate with that of Fig. 3(b). For the same parameters, we can obtain another equilibrium state called "double-core vortex lattice" in Fig. 1, where a vortex lattice of component 2 is made by pairs of vortices with the same circulation; vortices in component 1 surround those pairs. Therefore, various metastable structures will appear in this parameter region.

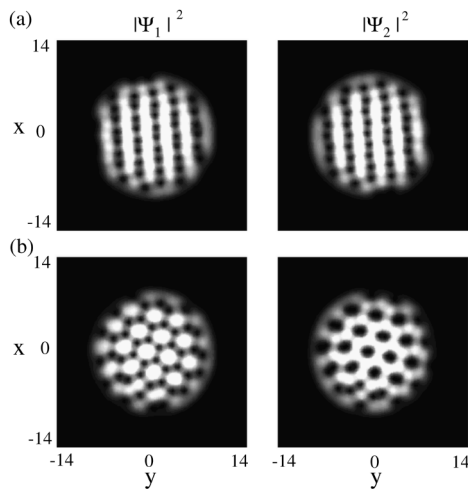For the strongly phase-separated region $\delta > 1$, the density peaks of the same spin component, at which the other-component vortices are located, merge further, re-sulting in the formation of vortex sheets; a typical example is shown in Fig. 4(a). Singly quantized vortices line up in sheets, and the sheets of component 1 and 2 are interwoven alternately from the center to the outward. Figure 4(b) shows that each superfluid velocity v_i ($i = 1, 2$) jumps at the vortex sheet, following approximately the velocity of solid-body rotation. In the region $\delta > 1$, even though the value of δ is changed, the total density is fixed by the Thomas-Fermi distribution with $\delta = 1$.

The stationary vortex sheet has been observed in rotating superfluid ^{3}He-A [16], where vortices are bounded to a topologically stable domain wall soliton across which the unit vector representing the direction of the orbital angular momentum of the Cooper-pair faces oppositely. As discussed in superfluid ^{3}He-A, the equilibrium distance between the sheets of component 1 and component 2 is determined by the competition between the surface tension σ of the domain wall and the kinetic energy of the superflow [16]. In order to estimate that distance in two-component BECs, we consider a simple model shown in Fig. 4(c). In this model, each velocity is assumed to be constant between the vortex sheets of the *same* component; the value of v_i increases by $2\bar{\Omega}b$ across every sheet. The total density $\rho_T = |\Psi_1|^2 + |\Psi_2|^2$ is constant, and the domain boundary with the penetration depth $\Lambda (<b)$ is
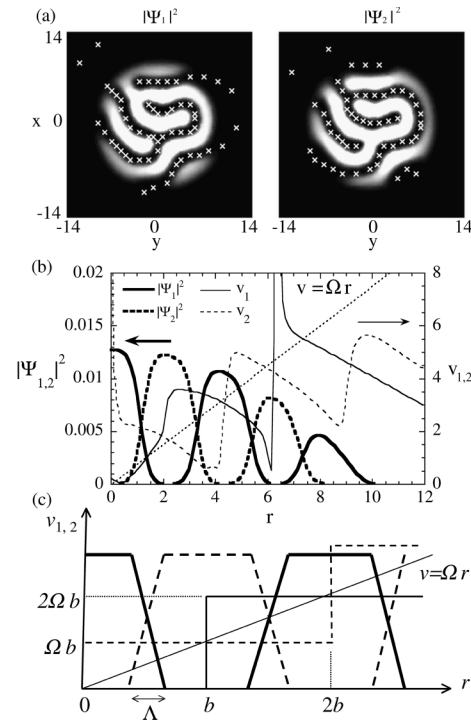

FIG. 4. (a) The density profiles of the condensates for $\bar{\Omega} = 0.75$ and $\delta = 1.1$. The vortex sheets are made up of chains of singly quantized vortices whose positions are marked by $\times$. (b) The density profile of Ψ_1 and Ψ_2 in the radial component, and the corresponding velocity profile. The velocity of solid-body rotation is shown by the dotted line. (c) Schematic illustration of the model of the vortex sheet state.

FIG. 3. The density profiles of the condensates Ψ_1 and Ψ_2 for $\bar{\Omega} = 0.7$ and $\delta = 1$. The profiles (a) and (b) are obtained by the numerical simulation starting from different trial wave functions. The energy deference between these states is $\Delta E \sim 10^{-5}$.

approximated by the linear profile. We calculate the free energy $F = E - \Omega L_z$ in the range $0 < r < 2b$, the sheet distance b being determined so as to minimize F per unit area. First, the penetration depth Λ is determined by minimizing the surface tension σ of a single domain wall with respect to Λ [10], which is the sum of the quantum pressure energy $E_{qp}/2\pi b \approx (\rho_T/2\Lambda)$ and the interaction energy in the overlap region $E_{int}/2\pi b = (\delta - 1)\Lambda \rho_T^2/12$; we thus obtain $\Lambda_p = \sqrt{6/C(\delta-1)\rho_T}$. Then, the surface tension is written as $\sigma = \rho_T^{3/2}\sqrt{C(\delta-1)/6}$. Second, the flow energy per area (in rotating frame) is given by $(1/4\pi b^2)\int_0^{2b} d^2 r \sum_i \rho_i (v_i - \bar{\Omega}r)^2/2 = 29\rho_T \bar{\Omega}^2 b^2/768$, where $b \ll \Lambda_p$ is assumed. Thus, the free energy per unit area is written as

$$\frac{F}{4\pi b^2} = \frac{29\rho_T \bar{\Omega}^2 b^2}{768} + \frac{2\sigma}{b} + \frac{C\rho_T^2}{2}. \tag{1}$$

Minimizing this energy with respect to b, one obtains $b = (768\sigma/29\bar{\Omega}^2\rho_T)^{1/3} = (768/29\bar{\Omega}^2\Lambda_p)^{1/3}$. By using the Thomas-Fermi density at $r = 0$ with $\delta = 1$ as the value of ρ_T, the sheet spacing $b \propto (\delta-1)^{1/6}(1-\bar{\Omega}^2)^{1/12}/\bar{\Omega}^{2/3}$ is consistent with that of numerical solutions; for example, for parameters used in Fig. 4, we obtain $b = 3.09 b_{ho}$. The vortex sheet is expected in the region $b > \Lambda_p$ and $2b < R_{TF} = \sqrt{2/\sqrt{\pi\alpha}}$, as shown in the shaded region in Fig. 1. When $2b > R_{TF}$, i.e., b becomes comparable with the condensate size, the clear structure of sheets vanishes.

Finally, we comment on what structure could be observed in actual experimental conditions. The two-component BECs realized in JILA is a mixture of the states $|1, -1\rangle$ and $|2, 1\rangle$ of ^{87}Rb [5]. This mixture has the scattering lengths which have the same order, $a_{11}:a_{22}:a_{12} = 1:0.94:0.97$, i.e., $\delta \sim 1$ for equal particle numbers. Therefore, lattices with partially overlapping vortices of the same component, as shown in Fig. 3, are expected to be observed. The MIT group has observed the phase separation of a mixture of ^{23}Na BECs with $|1, 0\rangle$ and $|1, 1\rangle$ state [17], which has $\delta \gtrsim 1$ ($a_{11}:a_{22}:a_{12} = 1:1.035:1.035$). In addition, a mixture of ^{41}K and ^{87}Rb BECs reported recently [18] lies deeply in a phase-separate region. The vortex sheets should therefore be observed at high rotation frequencies.

In conclusion, we reveal a rich phase diagram of vortex states in rotating two-component BECs, even in the restricted parameter space $(\delta, \bar{\Omega})$. The structure of a vortex lattice is shown to depend sensitively on the rotation frequency. In particular, we find new phenomena such as double-core vortex lattices and interwoven serpentine vortex sheets. Use of different atomic masses and intra-component interactions will realize a coexistence system of vortices with different vortex-core sizes; such a situation may change the lattice structure shown in this

Letter. We plan to study a more detailed phase diagram and effects of the internal Josephson coupling on the vortex states.

[1] D. Vollhardt and P. Wölfle, *The Superfluid Phases of Helium 3* (Taylor & Francis, London, 1990); M. Krusius, J. Low Temp. Phys. **91**, 233 (1993).

[2] R. Joynt and L. Taillefer, Rev. Mod. Phys. **74**, 235 (2002); A. P. Mackenzie and Y. Maeno, *ibid.* **75**, 657 (2003).

[3] *Topological Defects and the Non-Equilibrium Dynamics of Symmetry Breaking Phase Transitions,* edited by Y. M. Bunkov and H. Godfrin (Kluwer Academic Publishers, Les Houches, 1999).

[4] K. W. Madison *et al.*, Phys. Rev. Lett. **84**, 806 (2000); J. R. Abo-Shaeer *et al.*, Science **292**, 476 (2001); P. C. Haljan *et al.*, Phys. Rev. Lett. **87**, 210403 (2001); E. Hodby *et al.*, Phys. Rev. Lett. **88**, 010405 (2002).

[5] D. S. Hall *et al.*, Phys. Rev. Lett. **81**, 1539 (1998).

[6] T.-L. Ho and V. B. Shenoy, Phys. Rev. Lett. **77**, 3276 (1996).

[7] B. D. Esry *et al.*, Phys. Rev. Lett. **78**, 3594 (1997).

[8] P. Öhberg and S. Stenholm, Phys. Rev. A **57**, 1272 (1998).

[9] H. Pu and N. P. Bigelow, Phys. Rev. Lett. **80**, 1130 (1998).

[10] E. Timmermans, Phys. Rev. Lett. **81**, 5718 (1998).

[11] E. J. Mueller and T.-L. Ho, Phys. Rev. Lett. **88**, 180403 (2002).

[12] T. Kita *et al.*, Phys. Rev. A **66**, 061601(R) (2002).

[13] M. Tsubota *et al.*, Phys. Rev. A **65**, 023603 (2002).

[14] The energy is analogous to that of a binary alloy, in which $N/2$ A atoms and $N/2$ B atoms are distributed on N lattice sites. At each site there is only n_{Ai} or n_{Bi} ($n_i = 0$ or 1) atom. Denoting the three kinds of interaction energies between the atoms as ϵ_A, ϵ_B, and ϵ_{AB}, the interaction energy of this system reads $\sum_{i,j}\{\epsilon_A n_{Ai}n_{Aj} + \epsilon_B n_{Bi}n_{Bj} + \epsilon_{AB}(n_{Ai}n_{Bj} + n_{Aj}n_{Bi})\}$. The replacement $s_i = n_{Ai} - n_{Bi}$ reduces this energy to const $+ \epsilon\sum_{i,j}s_i s_j$. When the coefficient $\epsilon = (\epsilon_A + \epsilon_B + \epsilon_{AB})/4 > 0$, the interaction is antiferromagnetic, while for $\epsilon < 0$ it is ferromagnetic. See, for example, K. Huang, *Statistical Mechanics* (Wiley, New York, 1987), 2nd ed., Chap. 14.

[15] Vortex stripes in a single-component condensate have been observed by P. Engels *et al.*, Phys. Rev. Lett. **89**, 100403 (2002), in a nonequilibrium situation in the presence of quadrupolar perturbation.

[16] Ü. Parts *et al.*, Phys. Rev. Lett. **72**, 3839 (1994).

[17] H.-J. Miesner *et al.*, Phys. Rev. Lett. **82**, 2228 (1999).

[18] G. Modugno *et al.*, Phys. Rev. Lett. **89**, 190404 (2002).